Computing transition rates for rare events: When Kramers theory meets the free-energy landscape

François Sicard[*]

Department of Chemical Engineering, University College London, Torrington Place, London WC1E 7JE, United Kingdom

Computing reactive trajectories and free-energy landscapes associated with rare-event kinetics is key to understanding the dynamics of complex systems. The analysis of the free-energy landscape on which the underlying dynamics takes place has become central to compute transition rates. In the overdamped limit, most often encountered in biophysics and soft condensed matter, the Kramers theory and its multidimensional extension derived by Langer have proved to be quite successful in recovering correct kinetics. However, the additional calculation to obtain rate constants in complex systems where configurational entropy is competing with energy is still challenging conceptually and computationally. Building on the Kramers theory and the metadynamics framework, we propose an expression for the rate in terms of the height of the free-energy barrier measured along the minimum free-energy path and an auxiliary measure of the configurational entropy in terms of the joint probability distribution of the reactive and nonreactive coordinates representing the slow modes of the system. We apply the formalism to three different problems where our approach shows good agreement with simulations and experiments and can present significant improvement over the Kramers-Langer's framework when slow entropic contribution, such as configurational entropy, predominates over enthalpic contribution.

I. INTRODUCTION

Since the seminal work of Hendrik A. Kramers in 1940 [1], the study of rare events has been a subject of considerable interest to several scientific communities [2–10]. These events are rare because the systems of interest have to overcome some barriers, which can either be of an energetic or an entropic nature. From a theoretical viewpoint, rate theories, such as transition-state theory [11] and Kramers theory [1,2] (KT), have been successful in providing the language, the intuition, and the foundation for the development of computational tools for studying barrier-crossing events. What is most attractive about rate theory is its simplicity. It states basically that to move from the *reactant* state to the *product* state, the system has to navigate itself to the transition state, which is a saddle point on the potential or free-energy (FE) surface. In many cases, one can also define the most probable transition path for the reaction, which for overdamped systems of interest here is simply the minimum FE path (MFEP).

Molecular dynamics (MD) simulations are now used on a regular basis to study the statistical properties of barrier-crossing events in the long-time limit [4–8]. In the context of rare events, the systems can present different FE minima, each one trapping the dynamics for a time that can be long compared to fast bond vibrations, until a thermally activated jump is eventually performed toward another metastable or global minima. Ideally, a complete understanding of an activated process would encompass all of its kinetic aspects. However, there is often a wide gap between the timescale of the transition of interest and the timescale accessible with simulations, and one is content with reconstructing the geometric

pathways and their FE profiles [12,13]. To do so, a number of different computational approaches were introduced in the past few decades, sometimes designed for the purpose and sometimes borrowed from different disciplines [10]. Nevertheless, it remains necessary to asses the reliability of these methods with comparison to appropriate rate theory [14].

In the present work, we consider the overdamped limit most often encountered in biophysics and soft condensed matter [8,15], for which the Kramers theory and its multidimensional extension derived by Langer [16] have proved to be quite successful in recovering correct kinetics. Focusing on complex systems characterized with metastable states where entropy is competing with energy, we introduce a new approach to evaluate transition rates when configurational entropy [15,17,18] associated with slow nonreactive modes in the metastable basins makes the Kramers theory and its multidimensional extension fail. Building on KT and the metadynamics [19,20] (metaD) framework, the rate is first expressed in terms of the height of the FE barrier measured along the MFEP. We then define an auxiliary measure of the configurational entropy in terms of the joint probability distribution of the reactive and nonreactive coordinates representing the slow modes of the system along which the FE landscape is sampled [21].

II. THEORY

The starting point in the theory of barrier crossing under the influence of friction initiated by Kramers is the inertial Langevin equation with Markovian friction and random forces coupled to reaction coordinate motion [22]:

$$m\ddot{q} = -\frac{\partial V}{\partial q} - \gamma \dot{q} + R(t). \qquad (1)$$

———————
[*]Corresponding author: francois.sicard@free.fr

In Eq. (1), q represents the reaction coordinate, m is the reduced mass for the reaction coordinate, γ is the friction coefficient, and $V(q)$ is a potential of mean force (PMF). $R(t)$ is a random force with zero mean that satisfies the fluctuation-dissipation theorem [23]. Without loss of generality, we set $m = 1$ in the following. In principle, the Langevin equation can be constructed from MD simulations. For instance, the PMF can be computed using metaD or umbrella sampling simulations. KT is a valid approximation for real solvent as encountered in polymer physics and classic theories of nucleation and provides a unified framework for understanding how dynamics influence reaction rates [14]. In particular, the strong friction limit of interest here is where quantitative results from KT are most reliable. In this limit, the time evolution of the probability density $P(x, t)$ is governed by the Smoluchowski equation [1]

$$\frac{\partial P(q,t)}{\partial t} = -\frac{1}{\gamma}\frac{\partial}{\partial q}\left[\frac{\partial V}{\partial q}P(q,t) + \frac{1}{\beta}\frac{\partial P(q,t)}{\partial q}\right], \quad (2)$$

where the right-end term in Eq. (2) corresponds to the gradient of the probability flux J over the barrier

$$J = -\frac{1}{\gamma}e^{-\frac{V(q)}{k_B T}}\frac{\partial}{\partial q}\left[e^{\frac{V(q)}{k_B T}}P(q,t)\right], \quad (3)$$

considering the system is thermalized near the bottom of the well [1]. Following the original reasoning of Kramers [1], we assume a steady-state escape rate, k_{KT}, by considering a stationary situation for the the probability flux J, $\frac{\partial P}{\partial t} = 0$. For sufficiently high FE barrier the probability density follows the equilibrium relation $P(q) = P(q_0)\exp\{-[V(q) - V(q_0)]/k_B T\}$. Integrating Eq. (3) along the PMF and expanding about the transition state, q_T, yields

$$J = P(q_0)\frac{\sqrt{|V''(q_T)|}}{2\pi\gamma}e^{-\frac{V(q_T)-V(q_0)}{k_B T}}. \quad (4)$$

Rewriting $J = p\, k_{KT}$, with p the probability of the particle being inside the metastable well and k_{KT} the Kramers escape rate, we consider that the system is confined to a small neighborhood Ω_{q_0} around the minimum q_0 of the well. Expanding about this point, the probability of finding a particle in the well is

$$p = \int_{\Omega_{q_0}} P(x)dx = P(q_0)\sqrt{\frac{2\pi k_B T}{V''(q_0)}}. \quad (5)$$

This yields the Kramers escape rate

$$k_{KT} = \frac{\sqrt{V''(q_0) \times |V''(q_T)|}}{2\pi\gamma}e^{-\Delta V/k_B T}, \quad (6)$$

where $\Delta V = V(q_T) - V(q_0)$. The expression in Eq. (6) must account for the symmetric or asymmetric nature of the FE profile in the metastable states and the transition state. To do so, the PMF $V(q)$ in Eq. (1) can either be fitted with Gaussian or skew-Gaussian curve depending on the symmetric or asymmetric nature of the FE profile either in the metastable

well bottom or the transition state [15,24], respectively

$$V_{\text{sym}}(q) \propto e^{-(q-q_0)^2/2\sigma^2}, \quad (7)$$

$$V_{\text{asym}}(q) \propto V_{\text{sym}}(q)\left\{1 + \text{erf}\left[\frac{\alpha(q-q_0)}{\sqrt{2}\sigma}\right]\right\}, \quad (8)$$

with σ and α the parameters of the distributions. We can then rewrite Eq. (6) in the form of the expression originally derived by Kramers in the overdamped regime [1],

$$k_{KT} = \frac{\omega_0^{\text{eff}}\omega_T^{\text{eff}}}{2\pi\gamma}e^{-\Delta V/k_B T}, \quad (9)$$

where ω_0^{eff} and ω_T^{eff} represent the *effective* stiffnesses of the well and the barrier, respectively, modeled with the symmetric or asymmetric distributions in Eqs. (7) and (8). In Eq. (9), $\Delta V = V(q_T) - V(q_0)$ can either represent a potential energy difference, as originally considered by Kramers [1], or a FE difference, as considered thereafter.

The KT discussed above gives a physical derivation of the reaction rate constant, k_{KT}, in terms of the shape of the FE profile, which includes the full enthalpic and entropic contributions. This consideration comes closer to reality for a reaction with a FE landscape containing a large energy barrier and narrow valley between *reactants* and *products*, but it will be a poor approximation in the presence of slow nonreactive modes, such as configurational entropic contribution [14]. In such a case the standard KT fails and the slow mode dynamics must be treated explicitly on an equal footing with the mode along the reaction coordinate, as addressed within the multi-dimensional Kramers-Langer's framework (KLT) [16,25–27] with the escape rate

$$k_{KLT} = \frac{1}{2\pi}\left[\frac{\det H_V(q_0)}{|\det H_V(q_T)|}\right]^{1/2} h_T\, e^{-\Delta V/k_B T}. \quad (10)$$

In Eq. (10), $H_V(q_0)$ and $H_V(q_T)$ are the Hessian matrices of the potential energy function with respect to coordinates at the well bottom and the transition state, respectively, and h_T is a single positive root of the equation $\det[\hat{m}h + \hat{\gamma}h + V(q_T)] = 0$, where $\hat{m}$ and $\hat{\gamma}$ are the tensors of masses and friction coefficients, respectively [16,25,26].

Eventually, the *global* convergence of the multidimensional FE surface might even not be achieved within the metaD framework when *large* entropic fluctuations come into play and both KT and KLT fail. To overcome this limitation, we propose an expression for the rate constant in terms of the height of the free-energy barrier measured along the MFEP, $\mathcal{F}$, and an auxiliary measure of the configurational entropy, S^{conf}, in terms of the joint probability distribution of the reactive and nonreactive coordinates representing the slow modes of the system.

Since its introduction in 1981 by Kushick and Karplus in the context of macromolecules [17], a number of methods have been proposed in the literature to estimate the configurational entropy of complex systems [17,18,30–32]. We consider here the definition of the FE difference between two metastable basins $\mathcal{B}_i$ and $\mathcal{B}_j$, ΔF_{ij}^*, in terms of the joint probability distribution of the collective variables (CVs) representing the slow modes of the system along which the FE landscape is sampled [21]. The entropic contribution of the FE

surface can be assessed quantitatively,

$$\Delta F_{ij}^* = -k_B T \log\left(\frac{P_i}{P_j}\right),\tag{11}$$

where P_i and P_j are the probabilities of states i and j, respectively. The probability of each state is computed as the integral of the distribution within the FE basin it occupies on the CV-space sampled within the metaD framework,

$$P_i = \iint_{\mathcal{B}_i} f(C_1, C_2, \ldots)\, dC_1\, dC_2 \ldots,\tag{12}$$

where f is the joint probability density distribution function associated with the system FE, and $\{C_1, C_2, \ldots\}$ is the subset of CVs associated with the slow reactive and nonreactive coordinates. As the latter are predominantly associated with entropic barriers, they are not necessarily used as CVs within the accelerated MD framework considered to bias the simulation. The FE difference defined in Eq. (11) is not, in general, the exact FE difference between metastable states, which is a well-defined quantity not dependent on any choice of CV. Instead, it represents a surrogate expression, due to integration of probability in a smaller region than that of each metastable state, formally capturing the reactive and nonreactive coordinates representing the slow modes of the system.

Denoting $\Delta\mathcal{F}_{ij}$ the FE difference between the two metastable basins $\mathcal{B}_i$ and $\mathcal{B}_j$ measured along the MFEP, the difference in configurational entropy, $\Delta S_{ij}^{\mathrm{conf}}$, would be assessed as [32]

$$-T\Delta S_{ij}^{\mathrm{conf}} = \Delta\mathcal{F}_{ij} - \Delta F_{ij}^*.\tag{13}$$

Considering in Eq. (9) the auxiliary measure of the configurational entropy, the ratio k_i/k_j between the rates associated with the transition between two metastable basins $\mathcal{B}_i$ and $\mathcal{B}_j$ can be written as

$$\frac{k_i}{k_j} = k_{\mathrm{conf}}^{(ij)}\left(\frac{\omega_i}{\omega_j}\frac{\gamma_j}{\gamma_i}e^{-\Delta\mathcal{F}_{ij}/k_B T}\right),\tag{14}$$

with $k_{\mathrm{conf}}^{(ij)} = e^{\Delta S_{ij}^{\mathrm{conf}}/k_B} = e^{(\Delta F_{ij}^* - \Delta\mathcal{F}_{ij})/k_B T}$ a correction factor accounting for the difference in configurational entropy between the metastable basins. Given the definition on the FE difference in Eq. (11), the transition rate ratio assessed in Eq. (14) would represent a surrogate of the correct ratio whenever ΔF_{ij}^* is not the exact free-energy difference between metastable states. Substituting in Eq. (14) the FE differences, $\Delta\mathcal{F}_{ij}$ and ΔF_{ij}^*, between the metastable basins $\mathcal{B}_i$ and $\mathcal{B}_j$ with the FE difference, $\Delta\mathcal{F}_{i\mathcal{T}}$ and $\Delta F_{i\mathcal{T}}^*$, between the metastable basin $\mathcal{B}_i$ and the transition state $\mathcal{T}$ in Eqs. (13) and (11), we can rewrite Eq. (9) to assess the absolute transition rate as

$$k_i = k_{\mathrm{conf}}^{(i\mathcal{T})}\left(\frac{\omega_i \omega_T}{2\pi\gamma_i}e^{-\Delta\mathcal{F}_{i\mathcal{T}}/k_B T}\right),\tag{15}$$

with $k_{\mathrm{conf}}^{(i\mathcal{T})} = e^{(\Delta F_{i\mathcal{T}}^* - \Delta\mathcal{F}_{i\mathcal{T}})/k_B T}$. Eventually, the direct estimation of the absolute transition rate, k_i, can be determined if the reduced mass, m, and the effective friction coefficient, γ, defined in Eq. (1) are known [14]. As in *standard* KT, the parameters m and γ can be obtained from the equipartition theorem and clamped simulations, respectively, as discussed in Ref. [14]. The computation of the absolute transition rates

derived in Eq. (15) would then be subject to the reliability of Eq. (11), at least when configurational entropy is competing with energy, in the neighborhood of the transition state [33,34].

III. RESULTS AND DISCUSSION

In the following, we proceed with three illustrative applications of our approach, each with different levels of coarse-graining and entropic contribution. We focused our analysis on the calculation of the ratio of transition rates as it is encountered when comparing with equilibrium constant measured in biophysical experiments [35]. The details of the numerical simulations are given in the appendices. The first two examples show that our approach is in close agreement either with the *standard* Kramers theory or its multidimensional extension when a *truly* converged FE profile can be reconstructed within the metaD framework. In the last example, where configurational entropy associated with slow nonreactive modes competes significantly with the enthalpy of the system, Kramers-Langer's theory fails as the convergence of the FE profile is not achievable. Nevertheless, our approach based on a converged MFEP, even in highly entropic systems, and an auxiliary measure of configurational entropy in the vicinity of the MFEP could assess quantitatively the interplay between the thermodynamics and kinetic characteristics of the system.

A. Alanine dipeptide in water

The conformational transition between the different conformers of the solvated alanine dipeptide has been extensively used as a case study for several theoretical and computational investigations [6,36–39]. We performed well-tempered metaD (WT-metaD) atomistic simulations [40,41] using both torsional angles Φ and Ψ as CVs. The FE surface for this molecule is shown in Fig. 1(a). The location of the metastable basins and the height of the FE barriers are in agreement with those found in the literature [36,37]. While the full analysis of the transition rate ratio accounting for the competition between the two transition states, TS1 and TS2, in Fig. 1, can be achieved using Eq. (15), we focused our analysis on the conformational transition between conformers α and β over the lowest FE barrier (TS2 in Fig. 1). We determined the value of the FE difference along the MFEP shown in Fig. 1(a), $\Delta\mathcal{F}_{\alpha\beta}^0 = \mathcal{F}(\beta) - \mathcal{F}(\alpha) = -0.3 \pm 0.1\, k_B T$. The nonlinear least-squares Marquardt-Levenberg algorithm [29] was implemented to fit the effective stiffnesses $\omega_m = 4.9 \pm 0.1$ and $\omega_0 = 5.3 \pm 0.1$ at the bottom of the metastable (α) and equilibrium (β) basins, respectively, along the MFEP. Furthermore, the FE difference, $\Delta F_{\alpha\beta}^* = -0.3 \pm 0.1\, k_B T$, defined in Eq. (11) in terms of the probability distribution of Φ and Ψ, was computed considering the successive isosurfaces in the FE basins depicted in Fig. 1(a) as integration domains [cf. Eq. (12)]. Assuming that the effective friction coefficient, γ, in Eq. (15) remains unchanged in the transitions $\alpha \leftrightarrow \beta$, one obtains the transition rate ratio, $k_{\beta\to\alpha}/k_{\alpha\to\beta} = (6.0 \pm 1.4) \times 10^{-1}$. This result is in good agreement with the numerical ratio obtained with the atomistic unbiased MD simulations $k_{\beta\to\alpha}^{(\mathrm{num})}/k_{\alpha\to\beta}^{(\mathrm{num})} = (6.9 \pm 1.1) \times 10^{-1}$ (cf. details in Appendix A).
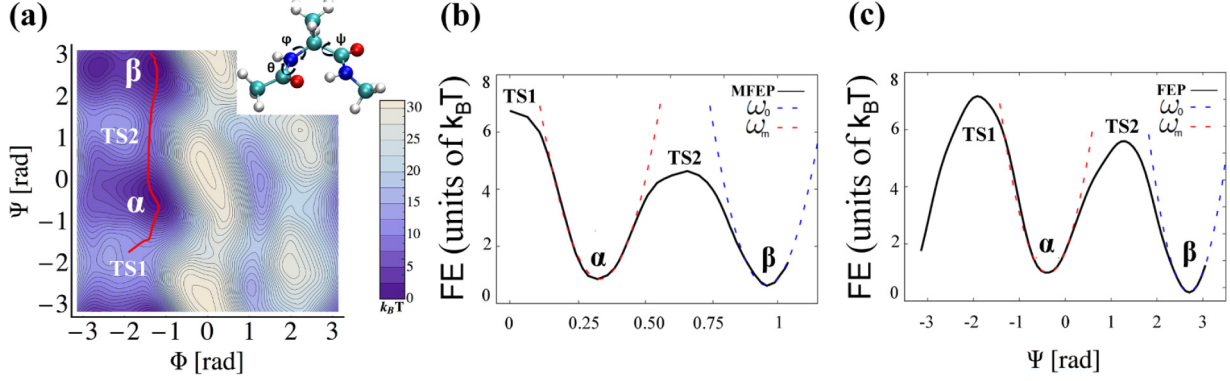
FIG. 1. (a) FE surface associated with the conformational transition between conformers α and β of solvated alanine dipeptide as a function of the two dihedral angles Φ and Ψ (see inset). The contour lines are every half $k_B T$. The typical MFEP obtained within the steepest descent framework [28] is shown in red along with the locations of the transition states (TS). (b) FE of solvated alanine dipeptide as a function of the progression along the typical MFEP (normalized to unity). (c) FE profile of solvated alanine dipeptide reconstructed along the dihedral angle Ψ obtained within the WT-metaD framework. The nonlinear least-squares Marquardt-Levenberg algorithm [29] was implemented to fit the effective stiffnesses ω_0 and ω_m, measured in the equilibrium (β) and metastable (α) states, respectively.

For comparison, the transition rate ratio, $k_{\beta \to \alpha}^{(KT)}/k_{\alpha \to \beta}^{(KT)}$, obtained within the *standard* KT in Eq. (9) was estimated. Figure 1(c) shows the FE profile of the system projected along the dihedral angle Ψ reconstructed within the WT-metaD framework. We determined the value of the FE difference along the FE profile, $\Delta F_{\alpha\beta}^0 = -0.6 \pm 0.1 \, k_B T$, and the effective stiffnesses $\omega_m = 4.8 \pm 0.1$ and $\omega_0 = 5.3 \pm 0.1$ at the bottom of the metastable (α) and equilibrium (β) basins, respectively. The *standard* KT yields $k_{\beta \to \alpha}^{(KT)}/k_{\alpha \to \beta}^{(KT)} = (6.0 \pm 1.0) \times 10^{-1}$, in close agreement with Eq. (14) and the numerical ratio obtained with the atomistic unbiased MD simulations.

B. Linear DNA denaturation bubble

The cooperative opening and closure of a sequence of DNA consecutive base pairs (bps) is central in biological mechanisms [8,42–46]. From a theoretical point of view, the double strand DNA (dsDNA) segments are considered to be in a low-entropy state and to carry the enthalpic contributions from the bound bps, whereas the flexible single-strand DNA (ssDNA) denaturation bubbles correspond to entropy reservoirs [42]. We performed coarse-grained WT-metaD and Brownian simulations using the width ρ_{max} of the bubble defined in Fig. 2(a) as CV. To explore the slow nonreactive mode associated with the entropic evolution of the DNA bubble within the metastable basin (op), we followed the evolution of the minimal twist angle, Φ_{min}, inside the bubble [8,47] along with the reactive coordinate ρ_{max} [cf. Fig. 2(b)]. The analysis of the FE surface associated with the bubble closure and opening mechanisms, as shown in Fig. 2(a), allowed us to determine the value of the FE difference measured along the MFEP (normalized to unity) depicted in Fig. 2(a), $\Delta \mathcal{F} = \mathcal{F}(\text{op}) - \mathcal{F}(\text{cl}) = 9.0 \pm 0.1 \, k_B T$. The nonlinear least-squares Marquardt-Levenberg algorithm [29] was implemented to fit the effective stiffnesses $\omega_m = 5.3 \pm 0.2$ and $\omega_0 = 64.2 \pm 2.1$ at the bottom of the metastable (op) and equilibrium (cl) basins, respectively, along the MFEP. Furthermore, to assess the value of the FE difference defined in Eq. (11) in term of the probability distribution of ρ_{max} and Φ_{min}, $\Delta F^* =$

$6.7 \pm 0.1 \, k_B T$, we considered the successive isosurfaces depicted in Fig. 2(a) as integration domains.

Considering the Rouse model [42] valid for flexible polymer chain, the effective friction coefficient, γ, in Eq. (15) depends on the number of opened bps, N_{bub}, in the DNA bubble. The typical size observed in the simulations, $N_{bub} \approx 10$ bps, yields the relation $\gamma_{op}/\gamma_{cl} \approx N_{bub}$ between the effective frictions in Eq. (14). We obtained the transition rate ratio, $k_{cl \to op}/k_{op \to cl} = (1.5 \pm 0.6) \times 10^{-3}$, as defined in Eq. (14), in close agreement with the numerical ratio obtained within the accelerated MD framework, $k_{cl \to op}^{(num)}/k_{op \to cl}^{(num)} = (1.8 \pm 0.4) \times 10^{-3}$ and the experimental times measured by Altan-Bonnet *et al.* [48] (cf. details in Appendix B).

For comparison, the transition rate ratio, $k_{cl \to op}^{(KT)}/k_{op \to cl}^{(KT)}$, obtained within the *standard* KT was estimated. Figure 2(c) shows the FE profile of the system projected along ρ_{max} reconstructed within the WT-metaD framework. We determined the value of the FE difference along the FE profile, $\Delta F^0 = 10.3 \pm 0.1 \, k_B T$, and the effective stiffnesses $\omega_m = 5.4 \pm 0.4$ and $\omega_0 = 64.3 \pm 1.9$ at the bottom of the metastable (op) and equilibrium (cl) basins, respectively. The *standard* KT defined in Eq. (9) yields $k_{cl \to op}^{(KT)}/k_{op \to cl}^{(KT)} = (4.0 \pm 0.7) \times 10^{-3}$, which differs by a factor 3 from the expression derived in Eq. (14). This overestimation would stem from the presence of slow nonreactive modes that must be treated explicitly [26,27].

To further assess the reliability of Eq. (14) when a *truly* converged FE surface is reconstructed within the WT-metaD framework, we estimated the transition rate ratio $k_{cl \to op}^{(KLT)}/k_{op \to cl}^{(KLT)}$ within the Kramers-Langer theory, which takes explicitly into account the slow nonreactive coordinate Φ_{min} along with the reactive coordinate ρ_{max}. Considering in Eq. (10) the FE difference measured along the MFEP, $\Delta \mathcal{F} = \mathcal{F}(\text{op}) - \mathcal{F}(\text{cl}) = 9.0 \pm 0.1 \, k_B T$, and the ratio $\{\det H_V(\text{cl})/ \det H_V(\text{op})\}^{1/2} = 1.0 \pm 0.4$, we obtained the transition rate ratio $k_{cl \to op}^{(KLT)}/k_{op \to cl}^{(KLT)} = (1.3 \pm 0.6) \times 10^{-3}$ in close agreement with Eq. (14) and the numerical ratio obtained within the accelerated MD framework (cf. details in Appendix B).
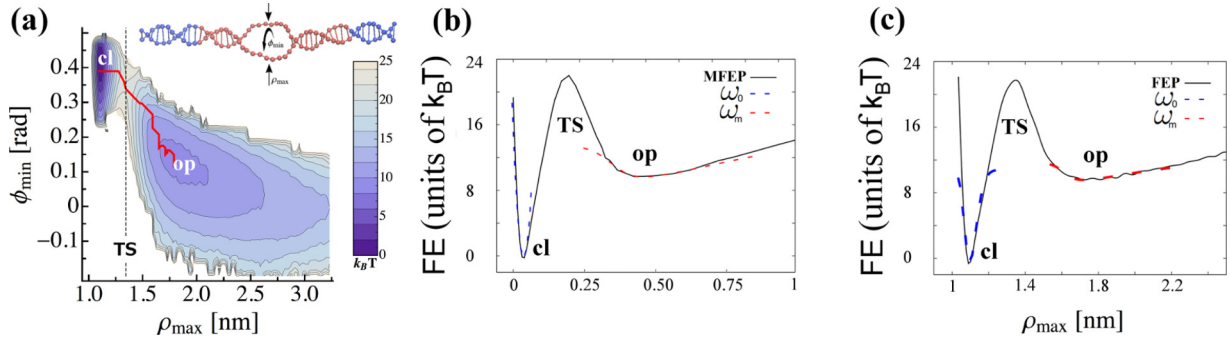
FIG. 2. (a) FE surface associated with the DNA bubble closure and nucleation mechanism projected along the maximal distance between paired bases ρ_{max} and the minimal twist angle between successive paired bases, ϕ_{min} (see inset). The contour lines are every two k_BT. The two stable basins associated with the opened (op) and closed (cl) states of the DNA bubble and the typical MFEP obtained within the steepest descent framework [28] are shown (red). (b) FE of the DNA bubble as a function of the progression along the typical MFEP (normalized to unity). (c) FE profile of the system projected along ρ_{max} reconstructed within the WT-metaD framework. The nonlinear least-squares Marquardt-Levenberg algorithm [29] was implemented to fit the effective stiffnesses ω_0 and ω_m, measured in the equilibrium (cl) and metastable (op) states, respectively.

C. Circular DNA denaturation bubble

To conclude this analysis, we studied the cooperative opening and closure of the denaturation bubble in a negatively supercoiled DNA minicircle within the WT-metaD framework and using the width ρ_{max} of the bubble as CV. As discussed in the previous example, we explore the slow nonreactive mode associated with the entropic evolution of the DNA bubble within the metastable basin (op), following the evolution of the minimal twist angle, Φ_{min}, inside the bubble. Building on the recent work of Sicard *et al.* [47], we set the parameters of the system so that neither the computation of a *truly* converged FE profile, as shown in Fig. 1(c), nor the direct numerical estimation of the transition rate, $k_{op \to cl}^{(num)}$, were achievable within an accelerated MD framework (cf. details in Appendix C). Indeed, the flatness of the FE basin associated with large configurational entropy contribution associated with slow nonreactive modes in the opened state of the denaturation bubble *significantly* predominates over the

enthalpy contribution. In such a case, the shape of the original FE surface could not be evenly maintained after the addition of the bias potential [4] and Kramers-Langer's theory fails.

Nevertheless, the convergence of the MFEP in Fig. 3(b) along with the convergence of the FE surface in its vicinity allowed us to determine the value the FE difference measured along the MFEP, $\Delta\mathcal{F}^0 = \mathcal{F}(op) - \mathcal{F}(cl) = -4.4 \pm 0.5\ k_BT$, and the effective stiffnesses $\omega_m = 69.5 \pm 3.1$ and $\omega_0 = 3.7 \pm 0.2$ at the bottom of the metastable (op) and equilibrium (cl) basins, respectively. Furthermore, we assessed the value of the FE difference defined in term of the probability distribution of ρ_{max} and Φ_{min}, $\Delta F^* = -8.6 \pm 0.4\ k_BT$, considering the successive isosurfaces in the FE basins depicted in Fig. 3(a) as integration domains.

Considering the typical size of the DNA bubble observed in the simulations, $N_{bub} \approx 12$ bps, we determined the parameter $\gamma_{op}/\gamma_{cl} \approx N_{bub}$ and obtained the transition rate ratio, $k_{cl \to op}/k_{op \to cl} = (1.0 \pm 0.4) \times 10^6$. This result is consistent
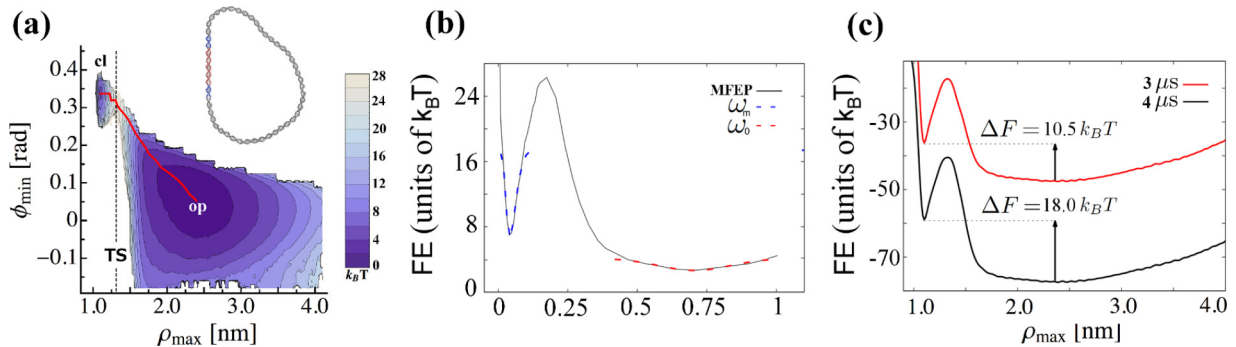

FIG. 3. (a) FE surface associated with the circular DNA bubble closure or nucleation mechanism projected along the maximal distance between paired bases ρ_{max} and the minimal twist angle between successive paired bases, ϕ_{min}. The contour lines are every two k_BT. The two stable basins associated with the opened (op) and closed (cl) states of the DNA bubble and the typical MFEP obtained within the steepest descent framework [28] are shown (red). (b) FE of the circular DNA bubble as a function of the progression along the typical MFEP (normalized to unity). The nonlinear least-squares Marquardt-Levenberg algorithm [29] was implemented to fit the effective stiffnesses ω_0 and ω_m, measured in the equilibrium (op) and metastable (cl) states, respectively. (c) Temporal evolution of the FE profile of the system along ρ_{max} reconstructed in the WT-metaD simulation. The convergence of the FE profile could not be achieved due to large entropic fluctuations. The FE profiles are shifted arbitrarily along the ordinate axis for clarity.

with the *inversion* of the thermodynamic stability of the system with respect to opened and closed DNA states, characteristic of the predominant stability of the *long-lived* denaturation bubble in supercoiled DNA [47]. Furthermore, the direct estimation of the transition rate $k_{\mathrm{cl}\to\mathrm{op}}^{(\mathrm{num})} = (204 \pm 25)$ s^{-1}, obtained within the accelerated MD framework, along with the computation of the ratio $k_{\mathrm{cl}\to\mathrm{op}}/k_{\mathrm{op}\to\mathrm{cl}}$ allowed us to assess the value of $k_{\mathrm{op}\to\mathrm{cl}}^{(\mathrm{num})} = (204 \pm 106)$ μs^{-1} (cf. details in Appendix C).

IV. CONCLUSION

In this paper we discussed the theoretical background and algorithmic details to compute the transition rates of complex systems when slow nonreactive modes, such as configurational entropy contribution, come into play and significantly predominate over the enthalpy contribution. In such a case, Kramers theory and its multidimensional extension can fail when the convergence of the FE profile is not achievable within the accelerated MD framework. To overcome this limitation, we proposed an alternative expression for the rate in terms of the height of the FE difference measured along a *truly* converged MFEP and an auxiliary measure of the configurational entropy in terms of the joint probability distribution of the reactive and nonreactive coordinates representing the slow modes of the system.

We considered three illustrative applications presenting different level of coarse-graining and entropic contribution. Our approach appears to be in close agreement either with the standard Kramers theory or its multidimensional extension when a truly converged FE profile is reconstructed within the metaD framework. In the limit where configurational entropy associated with slow nonreactive modes competes significantly with the enthalpy of the system, the shape of the original FE landscape cannot be *evenly* maintained within the accelerated MD framework. Nevertheless, our approach could assess quantitatively the interplay between the thermodynamics and kinetic characteristics of such complex systems.

Finally, let us comment on the dependence of the measure of the configurational entropy contribution on the choice of the auxiliary CVs associated with the slow nonreactive modes. Similarly to the metaD framework used to explore the FE landscape of complex systems, the reliability of our approach is strongly influenced by the choice of the auxiliary CVs considered in Eq. (12). To overcome such limitations, one could consider the potential energy of the system as an auxiliary CV as recently explored by Salvalaglio and coworkers [49], within the metaD framework, to break down FE surfaces into their entropic and enthalpic components. Eventually, one would compute rigorously the configurational entropy contribution and identify a complementary measure along an arbitrary chosen CV. This roadmap will be considered in the near future.

APPENDIX A: ALANINE DIPEPTIDE IN WATER

The metastable states of the solvated alanine dipeptide are differentiated by the values of the backbone dihedral angles Φ and Ψ, as defined in the main text, and are separated by activation FE barriers of $\approx$10 kJ/mol and $\approx$15 kJ/mol. We used a Langevin thermostat to enforce the temperature [51], a time step of 0.2 fs, AMBER03 forcefield [52] with TIP3P water model [53], and GROMACS 5.1 molecular dynamics code [54] patched with PLUMED 2.3 [55]. To reconstruct the FE surface, we performed WT-metaD atomistic simulations [40,41] using both torsional angles Φ and Ψ as CVs and a bias factor of 3 at 300 K. The initial Gaussian height was 1.25 kJ/mol, the width was 0.25 rad, and the deposition stride was 0.12 ps. A single alanine dipeptide molecule was kept in a solvated periodic cubic box of edge $\approx$3 nm. The LINear Constraint Solver (LINCS) algorithm [56] handled bond constraints while the particle-mesh Ewald scheme [57] was used to treat long-range electrostatic interactions. The nonbonded van der Waals cutoff radius was 0.8 nm.

To estimate the mean transition times between the metastable (α) and the equilibrium (β) states of the peptide, we ran a free MD simulation of 10 ns. We focused our analysis on the conformational transition between conformers α and β over the lowest FE barrier, as discussed in the main text. The statistics for $\tau_{\alpha\to\beta}^{(\mathrm{num})}$ and $\tau_{\beta\to\alpha}^{(\mathrm{num})}$ conformed to a Poisson distribution with means $\mu_{\alpha\to\beta} = (148 \pm 6) \times 10^{-3}$ ns and $\mu_{\beta\to\alpha} = (215 \pm 10) \times 10^{-3}$ ns and variance $\lambda_{\alpha\to\beta} = 106 \times 10^{-3}$ ns and $\lambda_{\beta\to\alpha} = 176 \times 10^{-3}$ ns, respectively. The statistics obey a two-sample Kolmogorov-Smirnov test [7] with p values equal to 0.96 and 0.88, respectively. This yields the numerical ratio $k_{\beta\to\alpha}^{(\mathrm{num})}/k_{\alpha\to\beta}^{(\mathrm{num})} = (6.9 \pm 1.1) \times 10^{-1}$.

APPENDIX B: LINEAR DNA DENATURATION BUBBLE

The characteristic times associated with cooperative opening and closure of a sequence of DNA consecutive base pairs (bps), composed of adenine (A), cytosine (C), guanine (G), and thymine (T), measured experimentally by Altan-Bonnet *et al.* [48] showed large bubble lifetimes of 20–100 μs and nucleation time of several ms. We used the DNA model of Refs. [8,46], where the mesoscopic DNA model consists in two interacting bead-spring chains each made of $N = 50$ beads (of diameter $a = 0.34$ nm) at position $\mathbf{r}_i$, with an AT-rich region of 30 bps in the middle and a GC region of 10 bps at each extremity. The Hamiltonian is $\mathcal{H} = \mathcal{H}_{\mathrm{el}}^{(1)} + \mathcal{H}_{\mathrm{el}}^{(2)} + \mathcal{H}_{\mathrm{tor}} + \mathcal{H}_{\mathrm{int}}$, where the first two contributions are elastic energies of the strands $j = 1, 2$ which include both stretching and bending energies,

$$\mathcal{H}_{\mathrm{el}}^{(j)} = \sum_{i=0}^{N-1} \frac{\kappa_s}{2}(r_{i,i+1} - a_{\mathrm{ref}})^2 + \sum_{i=0}^{N-1} \frac{\kappa_\theta}{2}(\theta_i - \theta_{\mathrm{ref}})^2. \quad \text{(B1)}$$

The stretching modulus, $a^2\beta_0\kappa_s = 100$, is a compromise between numerical efficiency and experimental values [58], where $\beta_0^{-1} = k_B T_0$ is the thermal energy, $T_0 = 300$ K is the room temperature, and $a_{\text{ref}} = 0.357$ nm. The bending modulus is large, $\beta_0\kappa_\theta = 600$, to maintain the angle between two consecutive tangent vectors along each strand θ_i to the fixed value $\theta_{\text{ref}} = 0.41$ rad. Each strand is thus modeled as a freely rotating chain [59]. The third and fourth terms of $\mathcal{H}$ are the torsional energy and hydrogen-bonding interactions, respectively. The torsional energy is modeled by a harmonic potential

$$\mathcal{H}_{\text{tor}} = \sum_{i=0}^{N-1} \frac{\kappa_{\phi,i}}{2}(\phi_i - \phi_{\text{ref}})^2, \tag{B2}$$

where ϕ_i is defined as the angle between two consecutive base-pair vectors $\boldsymbol{\rho}_i \equiv \mathbf{r}_i^{(1)} - \mathbf{r}_i^{(2)}$ and $\boldsymbol{\rho}_{i+1}$ ($\phi_{\text{ref}} = 0.62$ rad). The stacking interaction between base pairs is modeled through a $\kappa_{\phi,i}$ that depends on the value of the *bare* dsDNA torsional modulus κ_ϕ, and the distances between complementary bases, $\kappa_{\phi,i} = \kappa_\phi[1 - f(\rho_i)f(\rho_{i+1})]$, where

$$f(\rho_i) = \frac{1}{2}\left[1 + \text{erf}\left(\frac{\rho_i - \rho_b}{\lambda'}\right)\right], \tag{B3}$$

and $\rho_i = |\boldsymbol{\rho}_i|$. Hence, $\kappa_{\phi,i} = \kappa_\phi$ in the dsDNA state and $\kappa_{\phi,i} = 0$ in the ssDNA state. The actual values in the dsDNA state after equilibration, $\kappa_{\phi,\text{ds}}^*$, are, however, different from the prescribed values, κ_ϕ, due to thermal fluctuations and nonlinear potentials entering the Hamiltonian. The hydrogen-bonding interaction is modeled by a Morse potential

$$\mathcal{H}_{\text{int}} = \sum_{i=0}^{N-1} A\left(e^{-2\frac{\rho_i - \rho_{\text{ref}}}{\lambda}} - 2e^{-\frac{\rho_i - \rho_{\text{ref}}}{\lambda}}\right), \tag{B4}$$

where $\rho_{\text{ref}} = 1$ nm, $\lambda = 0.2$ nm, and $\beta_0 A = 8$ and 12 for AT and GC bonding, respectively, as in Refs. [8,46,60]. The fitted values for the dsDNA persistence length and the pitch are $\ell_{\text{ds}} \simeq 160$ bps and $p = 12$ bps for the relevant range of $\beta_0\kappa_\phi$ we are interested in, which are comparable to the actual dsDNA values ($\ell_{\text{ds}} \simeq 150$ bps and $p = 10.4$ bps). The ssDNA persistence length is $\ell_{\text{ss}} = 3.7$ nm, compatible with experimental measurement [61], even though in the upper range of measured values. The evolution of $\mathbf{r}_i(t)$ is governed by the overdamped Langevin equation, integrated using a Euler's scheme,

$$\zeta \frac{d\mathbf{r}_i}{dt} = -\nabla_{\mathbf{r}_i}\mathcal{H}(\mathbf{r}_j) + \xi(t), \tag{B5}$$

where $\zeta = 3\pi\eta a$ is the friction coefficient for each bead of diameter a with $\eta = 10^{-3}$ Pa s the water viscosity. The diffusion coefficient, $D_{\text{diff}} \equiv k_B T_0/3\pi\eta a$, thus takes into account the level of coarse-graining of the mesoscopic model involved in the kinetics associated with the smoothed free-energy landscape [62]. The random force of zero mean $\xi_i(t)$ obeys the fluctuation-dissipation relation $\langle \xi_i(t) \cdot \xi_i(t') \rangle = 6k_B T \zeta \delta_{ij}\delta(t - t')$. Lengths and energies are made dimensionless in the units of $a = 0.34$ nm and $k_B T_0$, respectively. The dimensionless time step is $\delta\tau = \delta t k_B T_0/(a^2\zeta)$, set to 5×10^{-4} ($\delta t = 0.045$ ps) for sufficient accuracy [8,46,60]. This set of parameters induces zipping velocities $v \approx 0.2$–2 bp/ns, compatible with experimental measurements [63].

To reconstruct the FE surface, we performed WT-metaD coarse-grained simulations with the width of the DNA bubble, $\rho_{\max}(t)$, as CV using the version 2.3 of the plugin for free-energy calculation, named PLUMED [55] According to the algorithm introduced by Barducci *et al.* [40,64] a Gaussian is deposited every 25 ps with initial height of 0.1 $k_B T$ and a bias factor of 5 at $T = 300$ K. The resolution of the recovered free-energy landscape is determined by the width of the Gaussians $\sigma = 0.1$ in units of the CV. As described in previous work [8], we put a wall at $\rho_{\max} \approx 4$ nm to prevent the system escaping from the metastable state (and therefore entering in the zipping regime, i.e., a far from equilibrium process [46,60]). To explore the *slow* entropic contribution associated with the DNA bubble metastable basin we chose to follow the evolution of the minimal twist angle $\Phi_{\min}$ inside the bubble [8], as described in the main text, reconstructed afterwards using the *reweighting technique* of Bonomi *et al.* [64].

To assess the reliability of our approach when a *truly converged* FE surface is reconstructed within the WT-metaD framework, we estimated the transition rate ratio $k_{\text{cl}\to\text{op}}^{(\text{KLT})}/k_{\text{op}\to\text{cl}}^{(\text{KLT})}$ within the Kramers-Langer theory, which takes explicitly into account the slow nonreactive coordinate $\Phi_{\min}$ along with the reactive coordinate $\rho_{\max}$ [cf. Eq. (10)]. As discussed in Ref. [27], we considered in Eq. (10) the FE difference measured along the MFEP, $\Delta\mathcal{F} = \mathcal{F}(\text{op}) - \mathcal{F}(\text{cl}) = 9.0 \pm 0.1 \, k_B T$. Considering the multidimensional elliptical asymmetric function to fit the parameters det $H_V(\text{cl})$ and det $H_V(\text{op})$,

$$V(q_1, q_2) \propto \left\{1 + \text{erf}\left[\alpha\left(q_1 - q_1^0\right)\right]\right\} \exp\left\{-\left[a_1\left(q_1 - q_1^0\right)^2 \right.\right.$$
$$\left.\left. + a_2\left(q_2 - q_2^0\right)^2 + a_{12}\left(q_1 - q_1^0\right)\left(q_2 - q_2^0\right)\right]\right\}, \tag{B6}$$

we computed the ratio $\{\det H_V(\text{cl})/\det H_V(\text{op})\}^{1/2} = 1.0 \pm 0.4$. We obtained the transition rate ratio $k_{\text{cl}\to\text{op}}^{(\text{KLT})}/k_{\text{op}\to\text{cl}}^{(\text{KLT})} = (1.3 \pm 0.6) \times 10^{-3}$ in close agreement with our approach and the numerical ratio obtained within the accelerated MD framework.

We extended the Metadynamics scope [4,6,7] to estimate the mean transition times between the metastable (op) and the equilibrium (cl) states of the DNA bubble. WT-metaD was performed using the width $\rho_{\max}$ as CV. Unlike in the FE surface reconstruction, no wall was added along the CV $\rho_{\max}$ in that case. We denote by τ the mean transition time over the barrier from the states and by τ_M the mean transition time for the metadynamics run. The latter changes as the simulation progresses and is linked to the former through the acceleration factor $\alpha(t) \equiv \langle e^{\beta V(s,t)} \rangle_M = \tau/\tau_M(t)$, where the angular brackets $\langle \ldots \rangle_M$ denote an average over a metadynamics run confined to the metastable basin, and $V(s, t)$ is the metadynamics time-dependent bias. To avoid depositing bias in the transition state region, we increase the time lag between two successive Gaussian depositions in the WT-metaD framework [6,7] to 700 ps and decrease the bias factor to 3. The statistics for $\tau_{\text{op}\to\text{cl}}^{(\text{num})}$ and $\tau_{\text{cl}\to\text{op}}^{(\text{num})}$ conformed to a Poisson distribution with means $\mu_{\text{op}\to\text{cl}} = 121 \pm 12 \, \mu s$ and $\mu_{\text{cl}\to\text{op}} = 67 \pm 8$ ms and variance $\lambda_{\text{op}\to\text{cl}} = 110 \, \mu s$ and $\lambda_{\text{cl}\to\text{op}} = 67$ ms, respectively. The statistics obey a two-sample Kolmogorov-Smirnov test [7] with p values

equal to 0.86 and 0.65, respectively. This yields the numerical ratio $k_{\text{cl}\to\text{op}}^{(\text{num})}/k_{\text{op}\to\text{cl}}^{(\text{num})} = (1.8 \pm 0.4) \times 10^{-3}$.

APPENDIX C: CIRCULAR DNA DENATURATION BUBBLE

The circular DNA (cDNA) is described with the same DNA model used for the linear DNA in Appendix B, where the two single strands are modeled as freely rotating chains of $N = 246$ beads of diameter $a = 0.34$ nm with a AT-rich region of 30 bps clamped by a closed circular GC region of $(N - 30)$ bps. The size of these AT-rich regions was chosen so that it is larger than the size of the representative *long-lived* denaturation bubbles studied in this work. Based on the recent work of Sicard *et al.* [47], the dsDNA minicircle is described by a circular helix where a helical line of radius α coils around a torus of radius R in the x-y plane. The centers of the beads on each strand initially coincide with the surface of this torus in Cartesian space according to the equations

$$x_n^{(j)} = \left\{ \alpha \sin\left[n\frac{2\pi}{p} + \psi^{(j)} \right] + R \right\} \times \cos(n\theta)$$

$$y_n^{(j)} = \left\{ \alpha \sin\left[n\frac{2\pi}{p} + \psi^{(j)} \right] + R \right\} \times \sin(n\theta) \quad \text{(C1)}$$

$$z_n^{(j)} = \alpha \cos\left[n\frac{2\pi}{p} + \psi^{(j)} \right]$$

with $x_n^{(j)}$, $y_n^{(j)}$, and $z_n^{(j)}$ the Cartesian coordinates of bead n on strand j. The parameter $\psi^{(1)} = 0$ for the first strand and $\psi^{(1)} = \pi$ for the second strand. The cross-sectional radius α is set equal to half the equilibrium base-pair distance,

$\rho_{\text{ref}} = 1$ nm, considered in previous work [8,46]. The twist angle between two base pairs is defined as $\phi = 2\pi/p$, where $p = 12.3$ is the DNA pitch, i.e., the number of bps corresponding to one complete helix turn. For purposes of generating the initial conformations, the bending angle per axis segment between the centers of two consecutive bps is set initially at $\theta = 2\pi/N$. We constrained a sequence of 10 GC bps on each extremity of the AT-rich region to be aligned arbitrarily along the z axis. The superhelical densities $\sigma = \frac{Lk - Lk^0}{Lk^0} = \frac{\Delta Lk}{Lk^0}$ along with the sizes N of the minicircles was specifically chosen to tune the value of the excess of linking number $\Delta L_k < 1$ [47]. The parameter $Lk = 20$ represents the linking numbers of the cDNA molecule and Lk^0 is defined as $Lk^0 = N/p_0$, with $p_0 = 12.0$ the equilibrium pitch measured in the *open linear* states.

As discussed in Appendix B, we performed WT-metaD coarse-grained simulations with the width of the DNA bubble, $\rho_{\text{max}}(t)$, as CV to reconstruct the FE surface and to estimate the mean transition times between the metastable (op) and the equilibrium (cl) states of the DNA bubble. We considered the WT-metaD parameters used for the linear DNA, only increasing the bias factor to 20 for the thermodynamic analysis. The statistics for $\tau_{\text{cl}\to\text{op}}^{(\text{num})}$ conformed to a Poisson distribution with means $\mu_{\text{op}\to\text{cl}} = 4.9 \pm 0.6$ ms and variance $\lambda_{\text{op}\to\text{cl}} = 6.0$ ms. The statistics obeys a two-sample Kolmogorov-Smirnov test [7] with a p value equal to 0.71. However, the numerical estimation of the transition time $\tau_{\text{cl}\to\text{op}}^{(\text{num})}$ was not achievable within the metaD framework, as the shape of the original FE surface could not be evenly maintained after the addition of the bias potential due to *large* entropic fluctuations. Nevertheless, our approach allowed us to assess the transition rate ration and to estimate $\tau_{\text{cl}\to\text{op}} = 80 \pm 40$ min.

[1] H. A. Kramers, Brownian motion in a field of force and the diffusion model of chemical reactions, Physica **7**, 284 (1940).

[2] P. Hänggi, P. Talkner, and M. Borkovec, Reaction-rate theory: Fifty years after Kramers, Rev. Mod. Phys. **62**, 251 (1990).

[3] E. Weinan and E. Vanden-Eijnden, Transition-path theory and path-finding algorithms for the study of rare events, Annu. Rev. Phys. Chem. **61**, 391 (2010).

[4] Y. Xin, U. Doshi, and D. Hamelberg, Examining the limits of time reweighting and kramers's rate theory to obtain correct kinetics from accelerated molecular dynamics, J. Chem. Phys. **132**, 224101 (2010).

[5] G. Gobbo, A. Laio, A. Maleki, and S. Baroni, Absolute Transition Rates for Rare Events from Dynamical Decoupling of Reaction Variables, Phys. Rev. Lett. **109**, 150601 (2012).

[6] P. Tiwary and M. Parrinello, From Metadynamics to Dynamics, Phys. Rev. Lett. **111**, 230602 (2013).

[7] M. Salvalaglio, P. Tiwary, and M. Parrinello, Assessing the reliability of the dynamics reconstructed from metadynamics, J. Chem. Theory Comput. **10**, 1420 (2014).

[8] F. Sicard, N. Destainville, and M. Manghi, Dna denaturation bubbles: Free-energy landscape and nucleation/closure rates, J. Chem. Phys. **142**, 034903 (2015).

[9] H. Mökkönen, T. Ala-Nissila, and H. Jónsson, Efficient dynamical correction of the transition state theory rate estimate for a flat energy barrier, J. Chem. Phys. **145**, 094901 (2016).

[10] F. Pietrucci, Strategies for the exploration of free energy landscapes: Unity in diversity and challenges ahead, Rev. Phys. **2**, 32 (2017).

[11] D. G. Truhlar, B. C. Garrett, and S. J. Klippenstein, Current status of transition-state theory, J. Phys. Chem. **100**, 12771 (1996).

[12] M. Mills and I. Andricioaei, An experimentally guided umbrella sampling protocol for biomolecules, J. Chem. Phys. **129**, 114101 (2008).

[13] H. Yu, A. N. Gupta, X. Liu, K. Neupane, A. M. Brigley, I. Sosova, and M. T. Woodside, Energy landscape analysis of native folding of the prion protein yields the diffusion constant, transition path time, and rates, Proc. Natl. Acad. Sci. USA **109**, 14452 (2012).

[14] B. Peters, *Reaction Rate Theory and Rare Events,* 1st ed. (Elsevier, Amsterdam, 2017).

[15] D. De, A. Singh, and A. N. Gupta, Locating transition path region in the free energy landscape of protein folding, arXiv:1705.01246.

[16] J. S. Langer, Statistical theory of the decay of metastable states, Ann. Phys. **54**, 258 (1969).

[17] M. Karplus and J. N. Kushick, Method for estimating the configurational entropy of macromolecules, Macromolecules **14**, 325 (1981).

[18] P. H. Nguyen and P. Derreumaux, Configurational entropy: An improvement of the quasiharmonic approximation using configurational temperature, Phys. Chem. Chem. Phys. **14**, 877 (2012).

[19] A. Laio and M. Parrinello, Escaping free-energy minima, Proc. Nat. Acad. Soc. USA **99**, 12562 (2002).

[20] A. Laio and F. L. Gervasio, Metadynamics: A method to simulate rare events and reconstruct the free energy in biophysics, chemistry and material science, Rep. Prog. Phys. **71**, 126601 (2008).

[21] I. Gimondi and M. Salvalaglio, CO_2 packing polymorphism under pressure: mechanism and thermodynamics of the i-iii polymorphic transition, J. Chem. Phys. **147**, 114502 (2017).

[22] W. Coffey and Y. Kalmykov, *The Langevin Equation*, 3rd ed., World Scientific Series in Contemporary Chemical Physics (World Scientific, Singapore, 2012), Vol. 27.

[23] U. Marini, B. Marconi, A. Puglisiand, L. Rondoni, and A. Vulpiani, Fluctuation-dissipation: Response theory in statistical physics, Phys. Rep. **461**, 111 (2008).

[24] M. T. Woodside, J. Lambert, and K. S. D. Beach, Determining intrachain diffusion coefficients for biopolymer dynamics from single-molecule force spectroscopy measurements, Biophys. J. **107**, 1647 (2014).

[25] A. M. Berezhkovskii and V. Yu. Zitserman, Solvent slow-mode influence on chemical reaction dynamics: A multidimensional kramers-theory treatment, Chem. Phys. Lett. **172**, 235 (1990).

[26] A. M. Berezhkovskii, V. Yu. Zitserman, and A. Polimeno, Numerical test of kramers reaction rate theory in two dimensions, J. Chem. Phys. **105**, 6342 (1996).

[27] C. Wei and A. Pohorille, Flip-flop of oleic acid in a phospholipid membrane: Rate and mechanism, J. Phys. Chem. B **118**, 12919 (2014).

[28] C. Chen, Y. Huang, and Y. Xiao, Efficiently finding the minimum free energy path from steepest descent path, J. Chem. Phys. **138**, 164122 (2013).

[29] P. E. Gill and W. Murray, Algorithms for the solution of the nonlinear least-squares problem, SIAM J. Numer. Anal. **15**, 977 (1977).

[30] C. Peter, C. Oostenbrink, A. van Dorp, and W. van Gunsteren, Estimating entropies from molecular dynamics simulations, J. Chem. Phys. **120**, 2652 (2004).

[31] S. Cheluvaraja and H. Meirovitch, Calculation of the entropy and free energy by the hypothetical scanning Monte Carlo method: Application to peptides, J. Chem. Phys. **122**, 054903 (2005).

[32] L. Leuzzi and Th. M. Nieuwenhuizen, *Thermodynamics of the Glassy State*, 1st ed., World Scientific Series in Contemporary Chemical Physics (Taylor & Francis Group, CRC Press, Boca Raton, FL, 2007).

[33] L. D. Landau and E. M. Lifshitz, *Statistical Physics,* 3rd ed. (Butterworth-Heinemann, Oxford, UK, 1980).

[34] K. J. Laidler and M. C. King, The development of transition-state theory, J. Phys. Chem. **87**, 2657 (1983).

[35] S. W. Englander, N. R. Kallenbach, A. J. Heeger, J. A. Krumhansl, and S. Litwin, Nature of the open state in long polynucleotide double helices: Possibility of soliton excitations, Proc. Nat. Acad. Soc. USA **77**, 7222 (1980).

[36] W. Ren, E. Vanden-Eijnden, P. Maragakis, and E. Weinan, Transition pathways in complex systems: Application of the finite-temperature string method to the alanine dipeptide, J. Chem. Phys. **123**, 134109 (2005).

[37] J. Vymetal and J. Vondrasek, Metadynamics as a tool for mapping the conformational and free-energy space of peptides—The alanine dipeptide case study, J. Phys. Chem. B **114**, 5632 (2010).

[38] Y. Yonezawa, I. Fukuda, N. Kamiya, H. Shimoyama, and H. Nakamura, Free energy landscapes of alanine dipeptide in explicit water reproduced by the force-switching wolf method, J. Chem. Theory Comput. **7**, 1484 (2011).

[39] J. Cuny, K. Korchagina, C. Menakbi, and T. Mineva, Metadynamics combined with auxiliary density functional and density functional tight-binding methods: Alanine dipeptide as a case study, J. Mol. Model **23**, 72 (2017).

[40] A. Barducci, G. Bussi, and M. Parrinello, Well-Tempered Metadynamics: A Smoothy Converging and Tunable Free-Energy Method, Phys. Rev. Lett. **100**, 020603 (2008).

[41] J. F. Dama, M. Parrinello, and G. A. Voth, Well-Tempered Metadynamics Converges Asymptotically, Phys. Rev. Lett. **112**, 240602 (2014).

[42] T. Ambjornsson and R. Metzler, Binding dynamics of single-stranded dna binding proteins to fluctuating bubbles in breathing DNA, J. Phys.: Condens. Matter **17**, S1841 (2005).

[43] T. Ambjornsson, S. K. Banik, O. Krichevsky, and R. Metzler, Sequence Sensitivity of Breathing Dynamics in Heteropolymer DNA, Phys. Rev. Lett. **97**, 128105 (2006).

[44] J.-H. Jeon, J. Adamcik, G. Dietler, and R. Metzler, Supercoiling Induces Denaturation Bubbles in Circular DNA, Phys. Rev. Lett. **105**, 208101 (2010).

[45] J. Adamcik, J.-H. Jeon, K. J. Karczewski, R. Metzler, and G. Dietler, Quantifying supercoiling-induced denaturation bubbles in DNA, Soft Matter **8**, 8651 (2012).

[46] A. K. Dasanna, N. Destainville, J. Palmeri, and M. Manghi, Slow closure of denaturation bubbles in DNA: Twist matters, Phys. Rev. E **87**, 052703 (2013).

[47] F. Sicard, N. Destainville, P. Rousseau, C. Tardin, and M. Manghi, Control of DNA denaturation bubble nucleation to advance nano-biosensing, arXiv:1805.04287 [physics.bio-ph].

[48] G. Altan-Bonnet, A. Libchaber, and O. Krichevsky, Bubble Dynamics in Double-Stranded DNA, Phys. Rev. Lett. **90**, 138101 (2003).

[49] I. Gimondi, G. A. Tribello, and M. Salvalaglio, Building maps in collective variable space, J. Chem. Phys. **149**, 104104 (2018).

[50] http://www.archer.ac.uk

[51] G. Bussi, D. Donadio, and M. Parrinello, Canonical sampling through velocity rescaling, J. Chem. Phys. **126**, 014101 (2007).

[52] D. A. Case, T. E. Cheatham, T. Darden, H. Gohlke, R. Luo, K. M. Jr. Merz, A. Onufriev, C. Simmerling, B. Wang, and R. J. Woods, The amber biomolecular simulation programs, J. Comput. Chem. **26**, 1668 (2005).

[53] W. L. Jorgensen, J. Chandrasekhar, J. D. Madura, R. W. Impey, and M. L. Klein, Comparison of simple potential functions for simulating liquid water, J. Chem. Phys. **79**, 926 (1983).

[54] E. Lindahl, B. Hess, and D. Van Der Spoel, Gromacs 3.0: A package for molecular simulation and trajectory analysis, J. Mol. Model. **7**, 306 (2001).

[55] G. A. Tribello, M. Bonomi, D. Branduardi, C. Camilloni, and G. Bussi, Plumed 2: New feathers for an old bird, Comput. Phys. Commun. **185**, 604 (2014).

[56] B. Hess, H. Bekker, H. J. Berendsen, and J. G. Fraaije, Lincs: A linear constraint solver for molecular simulations, J. Comput. Chem. **98**, 1463 (1997).

[57] T. Darden, D. York, and L. Pedersen, Particle mesh ewald: An nlog(n) method for ewald sums in large systems, J. Chem. Phys. **98**, 10089 (1993).

[58] T. Hugel, M. Rief, M. Seitz, H. E. Gaub, and R. R. Netz, Highly Stretched Single Polymers: Atomic-Force-Microscope Experiments Versus *Ab-Initio* Theory, Phys. Rev. Lett. **94**, 048301 (2005).

[59] A. Y. Grosberg and A. R. Khokhlov, *Statistical Physics of Macromolecules* (AIP Press, Melville, NY, 1994).

[60] A. K. Dasanna, N. Destainville, J. Palmeri, and M. Manghi, Strand diffusion-limited closure of denaturation bubbles in DNA, Europhys. Lett. **98**, 38002 (2012).

[61] B. Tinland, A. Pluen, J. Sturm, and G. Weill, Persistence length of single-stranded DNA, Macromolecules **30**, 5763 (1997).

[62] T. Murtola, A. Bunker, I. Vattulainen, M. Deserno, and M. Karttunen, Multiscale modeling of emergent materials: Biological and soft matter, Phys. Chem. Chem. Phys. **11**, 1869 (2009).

[63] C. Bustamante, S. B. Smith, J. Liphardt, and D. Smith, Single-molecule studies of DNA mechanics, Curr. Opin. Struct. Biol. **10**, 279 (2000).

[64] M. Bonomi, A. Barducci, and M. Parrinello, Reconstructing the equilibrium boltzmann distribution from well-tempered meta-dynamics, J. Comput. Chem. **30**, 1615 (2009).